Biquintic G^2 surfaces via functionals

Kęstutis Karčiauskas[a] and Jörg Peters[b]
[a] Vilnius University [b] University of Florida

November 17, 2014

Abstract

Recently, it was shown that a bi-cubic patch complex with n-sided holes can be completed into a curvature-continuous (G^2) surface by n-sided caps of degree bi-5 that offer good and flexible shape [KP13]. This paper further explores the space of n-sided caps of degree bi-5 but focusing on functionals to set degrees of freedom and to optimally propagate and average out curvature from the bi-cubic complex.

1 Introduction

Tensor-product splines of degree bi-3 represent the simplest choice for creating curvature continuous surfaces for a regular grid-like layout. Several such regular grids can be joined into a bi-cubic C^2 surface complex leaving multi-sided holes to be filled. When the surfaces are to be completed by curvature-continuous (G^2) multi-sided blends, the construction of degree bi-5 in [KP13] is likely to be of least polynomial degree – unless the shape is compromised. The construction in [KP13] leverages several carefully-chosen reparameterizations and intermediate, structurally simpler 'guide surfaces' to, step-by-step, establish the surface shape by prolonging and distributing curvature from the bi-cubic complex into a multi-sided cap. By generating well-shaped n-sided curvature continuous surface caps for a wide variety of challenging input data, the construction established that the space of bi-5 patches is sufficiently rich for such high-end modelling.

The main point of this paper is to further explore the space of bi-5 constructions, but without intermediate guide surfaces. To control the many degrees of freedom that surface caps of degree bi-5 offer after enforcing smoothness, we tested a variety of functionals that act separately on each of the coordinates f of the surface cap and have the form

$$\mathcal{F}_\kappa f := \int_0^1 \int_0^1 \sum_{i+j=\kappa, i,j\geq 0} \frac{\kappa!}{i!j!} (\partial_s^i \partial_t^j f(s,t))^2 ds dt, \tag{1}$$

as well as their tensor-analogues $\mathcal{F}_\kappa^* f := \int_0^1 \int_0^1 (\partial_s^\kappa f(s,t))^2 + (\partial_t^\kappa f(s,t))^2 ds dt$. The functional $\mathcal{F}_4^*$ was used in [Loo04, LS08] and combinations $\mathcal{F}_2 + \lambda \mathcal{F}_1$ for various λ have been used to approximate functionals based on first and second fundamental forms, e.g. [HKD93, Gre94, Gre96, LGS99, WN01, Sar00] (the last applies also $\mathcal{F}_3$). Setting degrees of freedom by such functionals may be considered less predictable (see Fig. 1) than successive approximation via guide surfaces, since the effect of minimizing such a functional over a complex blend of splines is difficult to predict – and may even fail to yield well-distributed highlight lines as our extensive experiments for 3−sided caps revealed. However, for $n > 4$, we could always find *some* functional that achieved quality comparable to [KP13] over all test cases: $\mathcal{F}_4$ works well for caps of valence $n = 5$, $\mathcal{F}_5$ for $n = 6$, $\mathcal{F}_7$ for $n = 7$ and $\mathcal{F}_8$ for $n = 8$ and beyond. For $n = 3$, all tested functionals failed to yield satisfactory highlight lines, i.e. yielded poorly distributed highlight lines on at least one and typically many test cases. But we discovered a simpler guided construction whose quality is on par with [KP13].

Overview. Section 2 gives an overview of the cap construction. Section 3 provides the details and summarizes the algorithm. Section 4 focuses on the special case $n = 3$. Section 5 shows the result of the modeling with functionals for challenging input configurations, and compares the new approach to [KP13], [LS08], as well as to Catmull-Clark subdivision [CC78]. First, we review the literature.

1.1 Patch-based G^2 surface constructions in the literature

Curvature continuous n-sided surface cap constructions have to be able to locally model any and all quadratic expansions at the central n-valent extra-ordinary point – and some cubic expansions to match higher-order

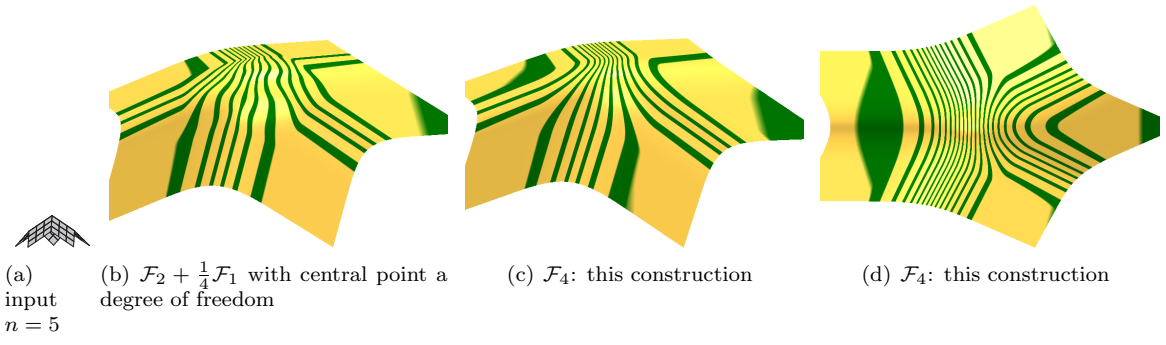

(a) input $n = 5$ (b) $\mathcal{F}_2 + \frac{1}{4}\mathcal{F}_1$ with central point a degree of freedom (c) $\mathcal{F}_4$: this construction (d) $\mathcal{F}_4$: this construction

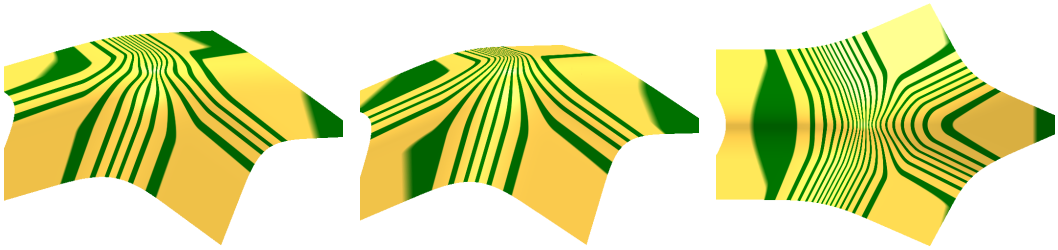

(e) $\mathcal{F}_2 + \frac{1}{4}\mathcal{F}_1$ with central point set to the Catmull-Clark limit point (f) [KP13] (guided) (g) $\mathcal{F}_8$

Figure 1: **Hit and miss with functionals.** While some (standard) functionals fail, $\mathcal{F}_4$ (but not $\mathcal{F}_8$) delivers for $n = 5$ highlight lines comparable to those in [KP13]. (*Artifacts such as bumps and oscillations are best visible on the screen when moving the object with respect to the light source. Therefore in* (d) *and* (g) *we chose a top view to reveal the difference in surface quality. Fig. 2 illustrates why we display highlight lines rather than Gauss curvature shading.*)

saddles. Otherwise we would simply extend the boundary data to a plane and generate a flat facet to satisfy curvature continuity. This requirement of 'flexibility' (local approximation order) forces a minimal polynomial degree for piecewise polynomial surface constructions. For example, flexible G^1 tensor-product caps based on quad meshes (and with possibly adjacent extraordinary points of valence $n \neq 4$) must have degree bi-3 or higher (and then 3×3 polynomial pieces per quad) to avoid flat spots when modeling higher-order saddles [PF09]. A similar lower bound theorem for G^2 surfaces is not yet proven, but it appears unlikely that a flexible G^2 cap of a C^2 bicubic B-spline complex, can be constructed exclusively with polynomial patches of degree bi-4; or that such caps can always be constructed using just one bi-5 patch per quad. For, while the bi-5 construction in [GZ99] is interesting from an algebraic point of view, the resulting shape generally disappoints, see Fig. 3.

Focusing on constructions that use a finite number of tensor-product spline pieces arranged in an unrestricted patch layout, the constructions of [GH95, CNG00] are high-degree rational and [YZ04] use root and exponential functions. (Flexibility with degree bi-3 can be achieved for 'polar configurations' via subdivision.

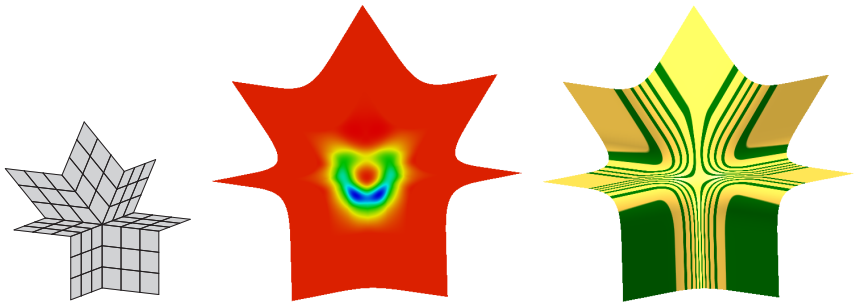

(a) input (b) Gauss curvature (c) highlight lines

Figure 2: **Surface interrogation.** Highlight lines (c) are often more revealing than Gauss curvature (b).

(a) input (b) [GZ99]

Figure 3: A G^2 scheme with poor highlight lines and visible distortion.

But here we focus on the more common 'star-like' configurations of Catmull-Clark subdivision [CC78], and allow only a finite number of polynomial pieces.) Among polynomial G^2 constructions using a single patch per quad, the degree can be as high as bi-18 [GH89]. The degree of [Ye97, Kic13] is bi-9. The constructions in [Pra97, Rei98] offer solutions of degree bi-6 – but only if their flexibility is restricted to second order. To attain third order flexibility, as is necessary to correctly model higher-order saddles, the constructions in [Pra97, Rei98] need to be of degree bi-9. The constructions of [Loo04, LS08] explore the space of degree bi-7 surfaces to fill an n-sided hole in a bi-3 spline complex. The formulas of [LS08] were derived by minimizing $\mathcal{F}_4^*$.

To separate *central points*, i.e. extraordinary points where more or less than four patches meet, or to reduce the sudden change in curvature at the transition between the cap and the surrounding bi-cubic surface, a number of surface constructions assume that the input control net is the result of *two or more* Catmull-Clark refinement steps. Such preprocessing may introduce shape problems due to the dominance of the hyperbolic terms [KPR04].

Guiding polynomials were introduced in [Pra97, Rei98] primarily to ensure C^2 continuity at the central point of the cap. Entire polynomials were also chosen as 'guide shapes' in the non-rational constructions [YZ04] and [Lev06]. Restricting the guides to be entire polynomials makes the resulting surfaces less flexible than using piecewise polynomial guides [Pet02]. For controlling shape, 'guided splines' [KP09] specifically advocate the use of piecewise guides over (global) optimization via functionals. The construction in [KP13] refined and improved this approach. Here, we revisit optimization via functionals, but only after careful reparameterization of the boundary data.

2 Construction Overview and Definitions

As illustrated in Fig. 4, our space of spline caps consists of n four-sided patches that each consist of 2×2 bi-5 pieces.

Definitions and Setup. We consider a network of quadrilateral facets or *quads* with vertices called control points. These control points are called regular points if they are surrounded by four quads and *star points* when surrounded by more or fewer than four quads. The analogous surface point, where more or fewer than four surface pieces (patches) meet, are called *central points*.

We assume, for simplicity of exposition, that each star point is surrounded by at least one layer of regular points. We denote as *cap-net* $\mathbf{c}$ the two-ring of one star point, i.e. the star point plus $6n$ points forming two layers of quads surrounding it. (Note that the second layer of quads is allowed to have star points.) The corresponding n-sided surface piece is called a surface *cap*. Fig. 5a displays a cap-net, and Fig. 5c displays an *extended cap-net* i.e. a cap-net plus one additional layer. This additional layer is not used for the construction of the cap but provides a surface ring (green in Fig. 5d) surrounding the cap for visual context and to assess the continuation of curvature from the surrounding complex into the cap.

Each 4×4 sub-grid of points of the network is interpreted as the B-spline control net of a bi-cubic tensor-product spline surface. The well-known formulas for converting from the B-spline to the Bernstein-Bézier form (*BB-form*; see e.g. [Far02, PBP02]) can be applied to the cap-net – except at star points. Along the boundary of a surface cap, this provides Hermite data in bi-degree 3 form (fine meshes in Fig. 5b,d). We refer to these Hermite data in the following as the *tensor-border* $\mathbf{b}$ (of depth 2 and degree 3) of the cap construction.

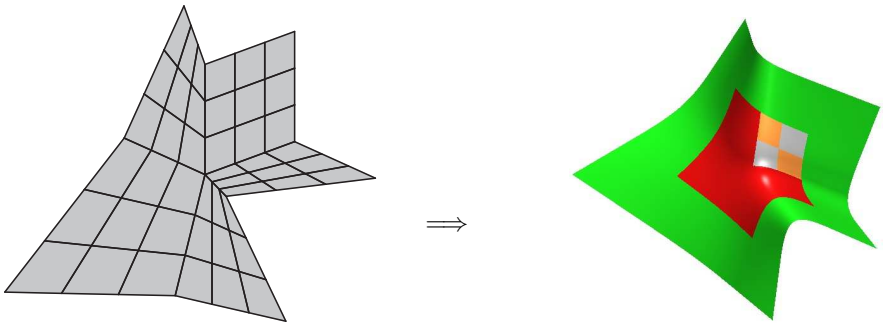

(a) Control net (b) Curvature continuous surface

.

Figure 4: Converting a **control net** into a curvature continuous surface of degree bi-5. (a) A net of control points with a star point of valence $n = 5$. The regular, grid-like part of the net defines (b) an outer (green) tensor-product spline layer of degree bi-3. The algorithm constructs the inner (red) cap. The upper right sector of the cap has its 2×2 pieces displayed.

(a) cap-net $\mathbf{c}$ (b) $\mathbf{l}$ (c) extended cap-net (d) surface ring

Figure 5: **Input.** (a) A cap-net $\mathbf{c}$ for $n = 5$ or, alternatively, (b) a corresponding tensor-border $\mathbf{b}$ of depth 2 represented as BB-form coefficients of degree 3. (c) Extended cap-net and (d) regular bi-3 surface layer (green) surrounding the tensor-border.

A tensor-product patch $\mathbf{f}$ of bi-degree d in Bernstein-Bézier form (BB-form) is defined by its BB-coefficients $\mathbf{f}_{ij}$ via

$$\mathbf{f}(u,v) := \sum_{i=0}^{d}\sum_{j=0}^{d} \mathbf{f}_{ij} b_i^d(u) b_j^d(v), \quad b_k^d(t) := \binom{d}{k}(1-t)^{d-k}t^k, \quad (u,v) \in \square := [0..1]^2,$$

i.e. all patches will be parameterized over the unit square. C^r continuity of surfaces can be achieved by G^r constructions, i.e. by relating adjacent surface pieces by reparameterization ρ so that, up to rth order, $\tilde{\mathbf{f}} = \mathbf{f} \circ \rho$. While the smoothness of the resulting surface can be expressed in the language of differential geometry, i.e. in terms of charts, it suffices, and is often more efficient, to express as agreement of one-sided r-jets along the boundary where two surface pieces are glued together. We use this approach in the following. Although ρ is just a change of variables, its choice is crucial for the properties of the surface cap.

Definition 1 *Two surface pieces* $\tilde{\mathbf{f}}$ *and* $\mathbf{f}$ *sharing a boundary curve* $\mathbf{e}$ *join* G^2 *if there exists a suitably oriented and non-singular reparameterization* $\rho : \mathbb{R}^2 \to \mathbb{R}^2$ *so that the jets* $\partial^k \tilde{\mathbf{f}}$ *and* $\partial^k(\mathbf{f} \circ \rho)$, $k = 0, 1, 2$, *agree along* $\mathbf{e}$.

Throughout, we will choose $\mathbf{e}$ to correspond to surface patch parameters $(u, 0 = v)$. Then the relevant Taylor expansion up to and including degree 2 of the reparameterization ρ with respect to v is

$$\rho = (u + b(u)v + \frac{1}{2}e(u)v^2, a(u)v + \frac{1}{2}d(u)v^2). \tag{2}$$

By the chain rule of differentiation, this yields the well-known constraints

$$\partial_v \tilde{\mathbf{f}} = a(u)\partial_v \mathbf{f} + b(u)\partial_u \mathbf{f}, \tag{3}$$

$$\partial_v^2 \tilde{\mathbf{f}} = a^2(u)\partial_v^2 \mathbf{f} + 2a(u)b(u)\partial_u\partial_v \mathbf{f} + b(u)^2\partial_u^2 \mathbf{f} + e(u)\partial_u \mathbf{f} + d(u)\partial_v \mathbf{f}. \tag{4}$$

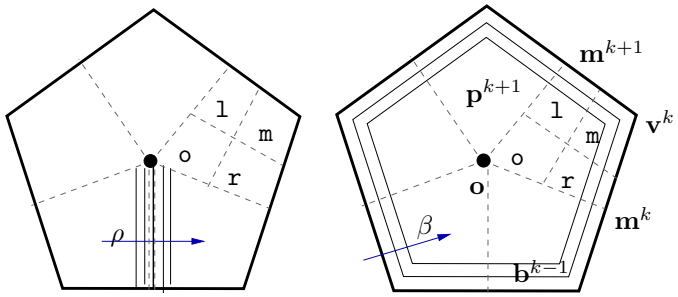

(a) inter-sector: Section 3.1 (b) tensor-border: Section 3.2

Figure 6: **Construction overview:** (The pentagon represents an n-sided hole within a bi-3 C^2 surface complex.) The surface cap $\mathbf{p}$ uses n spline patches $\mathbf{p}^k$, $k = 0, \ldots, n-1$. Each patch $\mathbf{p}^k$ consists of 2×2 pieces of polynomial degree bi-5 denoted by their superscripts $\mathtt{o}$, $\mathtt{r}$, $\mathtt{m}$, and $\mathtt{l}$ as $\mathbf{p}^{\mathtt{o},k}$, $\mathbf{p}^{\mathtt{r},k}$, $\mathbf{p}^{\mathtt{m},k}$, $\mathbf{p}^{\mathtt{l},k}$. The 'corners' of $\mathbf{p}$ (matching those of $\mathbf{b}$) are denoted by $\mathbf{v}^k$ and the 'edge-midpoints' of $\mathbf{p}$ (matching those of $\mathbf{b}$) by $\mathbf{m}^k$. The $k-1$st sector of the n-sided input tensor-border is denoted by $\mathbf{b}^{k-1}$.

3 Construction when $n > 4$

For this section, we assume that the valence of the star point is $n > 4$. The case $n = 3$ will receive special attention in Section 4. We construct the cap from n spline patches each of which consists of 2×2 pieces of polynomial degree bi-5 (see Fig. 6). This section explains the principles and main equations that yield the Algorithm in Section 3.3. The final implementation of surface caps can be reduced to forming a linear combination of tabulated generating functions weighted by the cap-net points $\mathbf{c}_j^k$, see Section 3.4.

3.1 Reparameterizing between sectors

Treating adjacent patches without bias for one side, we choose the reparameterization along the *inter-sector boundary* (cf. Fig. 6a) so that formula (2) simplifies to $a(u) := -1$ and $e(u) := b(u)\big(b'(u) - \frac{d(u)}{2}\big)$; i.e.

$$\rho = (u + b(u)\big(v + \frac{1}{2}(b'(u) - \frac{d(u)}{2})\big)v^2, -v + \frac{1}{2}d(u)v^2). \tag{5}$$

We name as $\rho^{\mathtt{o}}$ the reparameterization between the domains of $\grave{\mathbf{p}} := \mathbf{p}^{\mathtt{o},k-1}$ and $\acute{\mathbf{p}} := \mathbf{p}^{\mathtt{o},k}$ and as $\rho^{\mathtt{rl}}$ the reparameterization between the domains of $\grave{\mathbf{q}} := \mathbf{p}^{\mathtt{l},k-1}$ and $\acute{\mathbf{q}} := \mathbf{p}^{\mathtt{r},k}$ (see Fig. 7). We choose

$$\text{for } \rho^{\mathtt{o}} : b(u) := 2\mathtt{c}(1-u) + \frac{2}{3}\mathtt{c}u,\ d(u) := 0, \qquad \mathtt{c} := \cos\frac{2\pi}{n};$$

$$\text{for } \rho^{\mathtt{rl}} : b(u) := \frac{2}{3}\mathtt{c}(1-u)^2,\ d(u) := 0.$$

Since adjacent patches share the BB-coefficients along their common boundary, enforcing (3) locally between $\grave{\mathbf{p}}$ and $\acute{\mathbf{p}}$ by setting to zero each coefficient of the polynomial (in the boundary parameter u) that is the difference between the left side and the right side of (3). This yields a system of 6 linear equations. Enforcing (4) adds another 6 linear equations. Enforcing (3) and (4) locally between $\grave{\mathbf{q}}$ and $\acute{\mathbf{q}}$ yields another $7+8$ linear equations for a total of 27 linear equations. It is straightforward to compute the symbolic solution of this local system to express *dependent* BB-coefficients in terms of locally *independent* BB-coefficients as defined in Fig. 7b. We account for the interactions between the n such local systems of equations at a central point $\grave{\mathbf{p}}_{00}$ as follows.

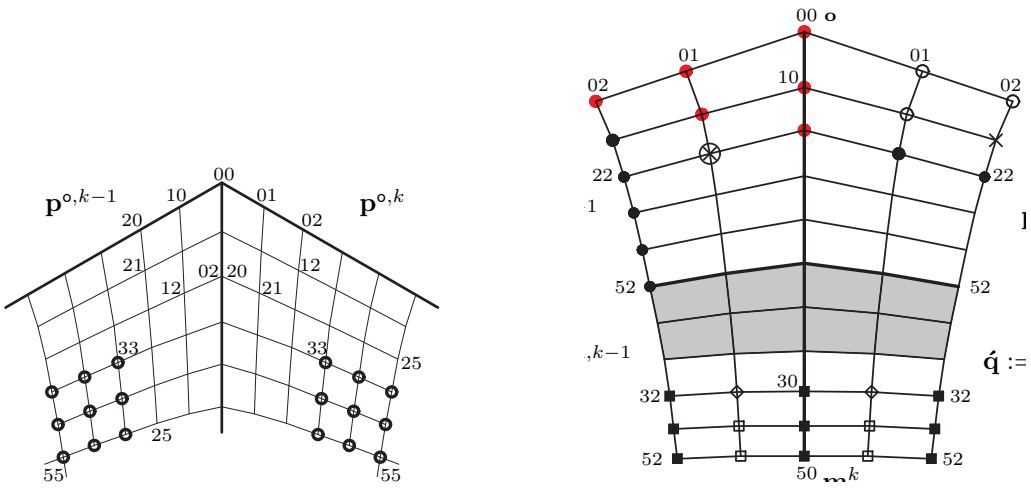

(a) rotationally-symmetric indexing (b) sector-symmetric indexing

Figure 7: **BB-coefficient indices.** (a) Indexing rotationally symmetric about the central point is appropriate for the full cap. Each 3×3 group of circled BB-coefficients determine a corner of $\mathbf{p}^{\circ,k}$ and hence the center of each C^2 2×2 macro-patch. (b) A G^2 *strip* of BB-coefficients $\{\grave{\mathbf{p}}_{ij}, \acute{\mathbf{p}}_{ij}, \grave{\mathbf{q}}_{ij}, \acute{\mathbf{q}}_{ij}\}$, $i=0,\ldots,5$, $j=0,\ldots,2$, determines the G^2 continuity between the two sectors. Here it is convenient to index the coefficients of $\grave{\mathbf{p}}$, $\acute{\mathbf{p}}$, $\grave{\mathbf{q}}$, $\acute{\mathbf{q}}$ symmetric with respect to the sector boundary so that $\grave{\mathbf{p}}_{ij}=\mathbf{p}^{\circ,k-1}_{ji}$ and $\acute{\mathbf{p}}_{ij}=\mathbf{p}^{\circ,k}_{ij}$. We choose as *dependent* the $3+4+2+1+12$ BB-coefficients marked by hollow circles, hollow squares, diamonds, the un-circled $\times$, and the unmarked grid points of $\grave{\mathbf{p}}$ and $\acute{\mathbf{p}}$. The unmarked grid points of $\grave{\mathbf{q}}$ and $\acute{\mathbf{q}}$ (in the grey-shaded area) are determined by C^2-extending $\grave{\mathbf{p}}$ to $\grave{\mathbf{q}}$, and $\acute{\mathbf{p}}$ to $\acute{\mathbf{q}}$. We denote as locally *independent* the BB-coefficients marked by red disks, the circled cross, solid black disks or solid black squares (see $\mathcal{P}_\rho$ in the text).

(i) We select the six BB-coefficients $\{\mathbf{p}^{\circ,0}_{lm}\}_{0\le l+m\le 2}$ that define the quadratic expansion of the *first sector* (index $k=0$) and then express the corresponding (initially independent) BB-coefficients of the other sectors recursively via (6)

$$\begin{aligned}
&\acute{\mathbf{p}}_{00} := \grave{\mathbf{p}}_{00}, \quad \acute{\mathbf{p}}_{10} := \grave{\mathbf{p}}_{10}, \quad \acute{\mathbf{p}}_{20} := \grave{\mathbf{p}}_{20}\ ;\\
&\acute{\mathbf{p}}_{01} := -\grave{\mathbf{p}}_{01} + 2\mathsf{c}\grave{\mathbf{p}}_{10} + 2(1-\mathsf{c})\grave{\mathbf{p}}_{00}\ ;\\
&\acute{\mathbf{p}}_{11} := -\grave{\mathbf{p}}_{11} + \frac{8\mathsf{c}}{5}\grave{\mathbf{p}}_{20} + 2\Big(1-\frac{11\mathsf{c}}{15}\Big)\grave{\mathbf{p}}_{10} - \frac{2\mathsf{c}}{15}\grave{\mathbf{p}}_{00}\ ;\\
&\acute{\mathbf{p}}_{02} := \grave{\mathbf{p}}_{02} - 5\mathsf{c}\grave{\mathbf{p}}_{11} + 4\mathsf{c}^2\grave{\mathbf{p}}_{20} + (5\mathsf{c}-4)\grave{\mathbf{p}}_{01} + \mathsf{c}\Big(9-\frac{26\mathsf{c}}{3}\Big)\grave{\mathbf{p}}_{10} + \Big(4-9\mathsf{c}+\frac{14\mathsf{c}^2}{3}\Big)\grave{\mathbf{p}}_{00}.
\end{aligned} \tag{6}$$

(ii) The assignment in each local system of

$$\begin{aligned}
\acute{\mathbf{p}}_{12} = {}& -2\mathsf{c}\grave{\mathbf{p}}_{21} + \grave{\mathbf{p}}_{12} + 2\mathsf{c}\acute{\mathbf{p}}_{21} + \Big(\frac{11\mathsf{c}}{3}-4\Big)\grave{\mathbf{p}}_{11} + \frac{4\mathsf{c}}{15}(12-11\mathsf{c})\grave{\mathbf{p}}_{20} + \Big(4-\frac{33\mathsf{c}}{5}+\frac{106\mathsf{c}^2}{45}\Big)\grave{\mathbf{p}}_{10}\\
&+ \frac{\mathsf{c}}{3}\grave{\mathbf{p}}_{01} + \frac{\mathsf{c}}{45}(26\mathsf{c}-27)\grave{\mathbf{p}}_{00}
\end{aligned} \tag{7}$$

leads globally to a circulant system for computing $\mathbf{p}^{\circ,k}_{12}$ (since $\mathbf{p}^{\circ,k-1}_{12}=\grave{\mathbf{p}}_{21}$ and $\mathbf{p}^{\circ,k}_{12}=\acute{\mathbf{p}}_{12}$, marked as $\otimes$, respectively $\times$ in Fig. 7b). This circulant system has a solution that is unique except for $n=6$, where one $\mathbf{p}^{\circ,k}_{12}$, say $\mathbf{p}^{\circ,0}_{12}$, is additionally free to choose. (The case $n=3$ leads to a singularity at the central point and is treated in Section 4 using a different construction.)

After applying (i) and solving (ii), the locally independent BB-coefficients in the union of all n G^2 strips that are still free to choose form the set (using the rotationally-symmetric indexing of Fig. 7a)

$$\mathcal{P}_\rho := \{\mathbf{p}^{\circ,k}_{2h}, \mathbf{p}^{\circ,0}_{lm}, \mathbf{p}^{k}_{\blacksquare}\}, \quad h=1,2,3,4,5,\ 0\le l+m\le 2, \quad k=0,\ldots,n-1,$$

(plus $\mathbf{p}^{\circ,0}_{12}$ if $n=6$). Here $\mathbf{p}^{k}_{\blacksquare}$ is the set of BB-coefficients marked as black squares in Fig. 7b. Since the subset $\mathbf{p}^{k}_{\blacksquare}$ will be determined by input tensor-border $\mathbf{b}$ in Section 3.2, enforcing the pairwise G^2 join of adjacent sectors leaves free $5n+6$ ($5n+7$ if $n=6$) BB-coefficients. By construction, we have the following lemma.

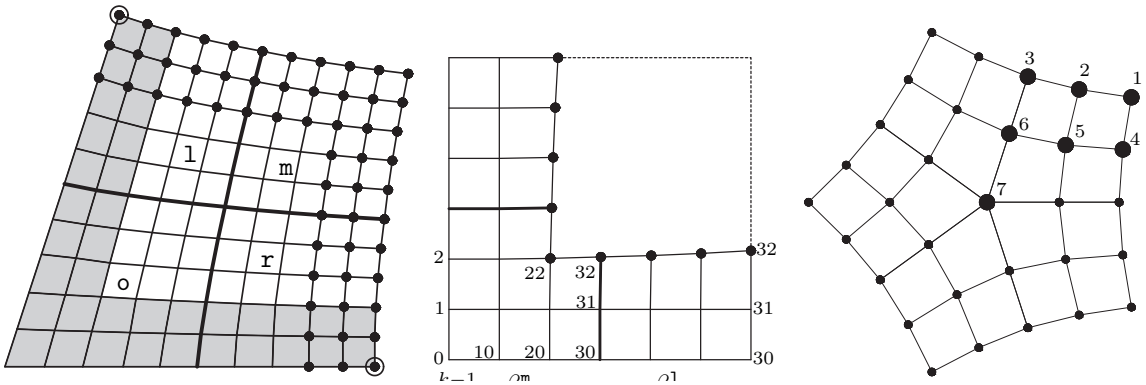

(a) Sector structure and labels (b) tensor-border reparameterization β (c) cap-net-indices; star point=$\mathbf{c}_7^k$

Figure 8: **Structure and labeling** (a) Four pieces of one sector (quad) covered by the spline-patch $\mathbf{p}^k$. The lower left corner is the central point. BB-coefficients marked as black disks match the tensor-border, BB-coefficients of the gray G^2 strips are involved in the inter-sector G^2 constraints. (b) Two-piece reparameterization β of the input tensor-border for the transition between the bi-3 C^2 tensor-border and the surface cap. Lower left corner corresponds to $\mathbf{v}^{k-1}$. (c) Indexing of the cap-net.

Lemma 1 *For any choice of BB-coefficients in $\mathcal{P}_\rho$, adjacent patches $\mathbf{p}^{k-1}$ and $\mathbf{p}^k$ join G^2 under the reparameterization ρ.*

3.2 Reparameterizing the tensor-border b

The G^1 and G^2 assignments at $\mathbf{m}^k$ (see the hollow boxes for (8) and diamonds $\diamond$ for (9) in Fig. 7b)

$$\grave{\mathbf{q}}_{i1} := \grave{\mathbf{q}}_{i0} + \frac{1}{4}(\grave{\mathbf{q}}_{i2} - \acute{\mathbf{q}}_{i2}), \quad \acute{\mathbf{q}}_{i1} := \grave{\mathbf{q}}_{i0} - \frac{1}{4}(\grave{\mathbf{q}}_{i2} - \acute{\mathbf{q}}_{i2}),\ i = 4, 5, \tag{8}$$

$$\begin{aligned}
\grave{\mathbf{q}}_{31} :=& \grave{\mathbf{q}}_{30} + \frac{1}{4}(\grave{\mathbf{q}}_{32} - \acute{\mathbf{q}}_{32}) + w_1(\grave{\mathbf{q}}_{52} - \acute{\mathbf{q}}_{52}) + w_2(\grave{\mathbf{q}}_{42} - \acute{\mathbf{q}}_{42}) + w_3(\grave{\mathbf{q}}_{50} - \grave{\mathbf{q}}_{40}),\\
\acute{\mathbf{q}}_{31} :=& \grave{\mathbf{q}}_{30} - \frac{1}{4}(\grave{\mathbf{q}}_{32} - \acute{\mathbf{q}}_{32}) - w_1(\grave{\mathbf{q}}_{52} - \acute{\mathbf{q}}_{52}) - w_2(\grave{\mathbf{q}}_{42} - \acute{\mathbf{q}}_{42}) + w_3(\grave{\mathbf{q}}_{50} - \grave{\mathbf{q}}_{40}),\\
w_1 :=& -\frac{\mathsf{c}}{96}, w_2 := \frac{\mathsf{c}}{96}, w_3 := \frac{\mathsf{c}}{30},
\end{aligned} \tag{9}$$

are incompatible with the C^2 tensor-border data. Therefore we define for each edge of one sector of the tensor-border $\mathbf{b}$, the reparameterization pieces $\beta^{\mathtt{m}}$ and $\beta^{\mathtt{l}}$ of degree bi-3 (see Fig. 8b). We choose the reparameterization to preserve the first cross-derivative along the border of the cap, i.e. $a(u) := 1$, $b(u) := 0$ in (2), and we enforce C^2 continuity between $\beta^{\mathtt{m}}$ and $\beta^{\mathtt{l}}$ and symmetry about the diagonal of $\beta^{\mathtt{m}}$. Then the choice

$$\beta^{\mathtt{m}}_{22} := \big(\frac{1}{3} + \frac{\mathsf{c}}{216}, \frac{1}{3} + \frac{\mathsf{c}}{216}\big),\ \beta^{\mathtt{m}}_{32} := \big(\frac{1}{2} + \frac{7\mathsf{c}}{1296}, \frac{1}{3} + \frac{\mathsf{c}}{72}\big),\ \beta^{\mathtt{l}}_{32} := \big(1, \frac{1}{3} + \frac{\mathsf{c}}{18}\big) \tag{10}$$

defines $\beta^{\mathtt{m}}$ and $\beta^{\mathtt{l}}$ up to second order along the tensor-border and makes compatible the prolongation of the tensor-border data and the smoothness constraints between sectors of the cap. Let β denote the reparameterization for the whole tensor-border and β^k its (identical) pieces, one for each sector.

Lemma 2 *The reparameterized tensor-border $\mathbf{b} \circ \beta$ is C^2 within each sector and adjacent pieces $\mathbf{b}^{k-1} \circ \beta^{k-1}$ and $\mathbf{b}^k \circ \beta^k$ join G^2 by satisfying* (8) *and* (9) *(see Fig. 7b).*

We complete the patches $\mathbf{p}^k$ so that they are internally C^2. This leaves free the set of $9n = (3 \times 3)n$ unconstrained BB-coefficients that determine the center of each $\mathbf{p}^k$ where its four pieces join (see circles in Fig. 7a). Combining Lemma 1 and Lemma 2 this yields overall curvature continuity.

Theorem 1 *For any choice of BB-coefficients*

$$\mathbf{p}^{\circ,k}_{2h}, \mathbf{p}^{\circ,0}_{lm}, \mathbf{p}^{\circ,k}_{ij}, \quad h = 1, 2, 3, 4, 5,\ 0 \le l + m \le 2,\ i, j = 3, 4, 5, \quad k = 0, \ldots, n-1,$$

(plus $\mathbf{p}_{12}^{\circ,0}$ if $n = 6$), the just-defined cap $\mathbf{p}$ is curvature continuous and joins the input patch complex with curvature continuity.

We can now succinctly state the full construction.

3.3 The Cap Construction

Input: A cap-net of $6n+1$ points $\mathbf{c}_j^k, j = 1, \ldots, 7$ with star point $\mathbf{c}_7 = \mathbf{c}_7^k$, $k = 0, \ldots, n-1$ of valence n (cf. Fig. 8c) – **or** – an n-sided tensor-border $\mathbf{b}$ of degree 3 and depth 2 (cf. Fig. 5b).

Output: (cf. Fig. 4) A surface cap $\mathbf{p}$ consisting of n spline patches $\mathbf{p}^k$, $k = 0, \ldots, n-1$. The patches $\mathbf{p}^{k-1}$ and $\mathbf{p}^k$ are joined G^2 and the cap joins with $\mathbf{b}$ both C^1 and G^2. Each spline patch $\mathbf{p}^k$ is internally C^2 and consists of 2×2 polynomial pieces $\mathbf{p}^{\circ,k}$, $\mathbf{p}^{\mathbf{r},k}$, $\mathbf{p}^{\mathbf{m},k}$, $\mathbf{p}^{\mathbf{l},k}$ of degree bi-5.

Algorithm (for $n > 4$, cf. Fig. 6)

1. Set the central point $\mathbf{p}_{00} = \mathbf{p}_{00}^{\circ,k}$ for all k to the limit point of Catmull-Clark subdivision [HKD93]

$$\mathbf{p}_{00} := \frac{n}{n+5}\mathbf{c}_7 + \sum_{i=0}^{n-1}(\gamma_5 \mathbf{c}_5^i + \gamma_6 \mathbf{c}_6^i), \quad \gamma_5 := \frac{1}{n(n+5)},\ \gamma_6 := \frac{4}{n(n+5)}.$$

2. Set the tensor-border of $\mathbf{p}$ to $\mathbf{b} \circ \beta$.

3. Expressing all dependent BB-coefficients in terms of $\mathbf{p}_{00}$ and the $9n + 5n + 5$ ($9n + 5n + 6$ if $n = 6$) BB-coefficients of

$$\mathcal{P} := \{\mathbf{p}_{2h}^{\circ,k}, \mathbf{p}_{lm}^{\circ,0}, \mathbf{p}_{ij}^{\circ,k}\}, \quad h = 1, 2, 3, 4, 5,\ 1 \le l + m \le 2,\ i, j = 3, 4, 5,$$

(plus $\mathbf{p}_{12}^{\circ,0}$ if $n = 6$), the surface is determined by minimizing

$$\min_{\mathcal{P}} \mathcal{F}_{\kappa(n)}\mathbf{p}, \qquad \kappa(n) := \begin{cases} n-1, \text{ for } n = 5, 6 \\ n, \text{ for } n = 7, 8 \\ 8, \text{ for } n > 8. \end{cases} \tag{11}$$

The valence-dependent choices of $\kappa(n)$ in (11) are the result of extensive comparisons (see Section 5).

3.4 Implementation via generating functions

The cap construction is linear and coordinate-wise. Due to the relatively short, explicit formulas for the dependent BB-coefficients in terms of the independent BB-coefficients, the construction steps of the Algorithm are simple and stable. With the central point set to the Catmull-Clark limit point of the cap-net, (11) requires only solving a linear system of size $N \times N$, where $N := 9n + 5n + 5$ ($14n + 6$ when $n = 6$). For all reasonable values of n, we have solved this system and computed seven *generating functions of the cap-net*. The final surface cap is a linear combination of these tabulated generating functions weighted by the cap-net points.

Specifically, since the Algorithm works for each coordinate separately, it can be applied to when all cap-net points have value 0, except for $\mathbf{c}_m^0 = 1$, for one of $m = 1, \ldots, 7$ (cf. Fig. 8c). This yields the scalar-valued bi-5 coefficients

$$h_{ij}^{k,m} \in \mathbb{R}, \quad k = 0, \ldots, n-1,\ m = 1, \ldots, 7,\ i, j \in \{0, \ldots, 5\},\ \text{where } h_{ij}^{0,7} = \ldots = h_{ij}^{n-1,7} \tag{12}$$

of the pieces attached to the central point. Then the central patches $\mathbf{p}^{\circ,\kappa}$, $\kappa = 0..n-1$ have the BB-coefficients

$$\mathbf{p}_{ij}^{\circ,\kappa} := h_{ij}^{0,7}\mathbf{c}_7 + \sum_{k=0}^{n-1}\sum_{m=1}^{6} h_{ij}^{k,m}\mathbf{c}_m^{\kappa-k}, \tag{13}$$

where the superscript of $\mathbf{c}_m^{\kappa-k}$ is interpreted modulo n. The remaining pieces are determined by the re-parameterized tensor-border and by C^2-extending the central pieces $\mathbf{p}^{\circ,\kappa}$.

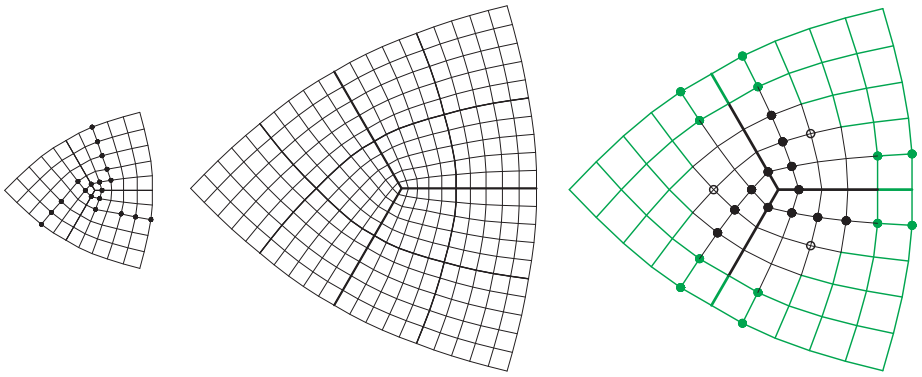

(a) $\mathbf{p}^\circ$ = inner cap

(b) map σ and layout of $\mathbf{p}$

(c) map $\bar{\sigma}$ and coefficients of the bi-5 guide $\mathbf{g}$

Figure 9: **Three-sided caps.** (a) BB-coefficients of the innermost pieces $\mathbf{p}^{\circ,k}$. (b) Structure of $\mathbf{p}$ and BB-coefficients of σ. (c) Independent points (after resolving inter-sector G^1 constraints) of the G^1 bi-5 guide $\mathbf{g}$ are marked as bullets superimposed on the BB-coefficients of $\bar{\sigma}$.

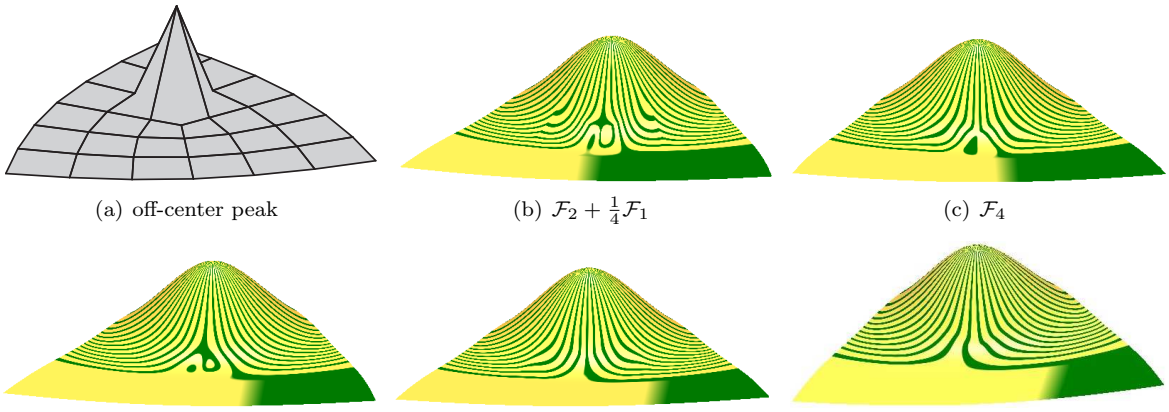

(a) off-center peak

(b) $\mathcal{F}_2 + \frac{1}{4}\mathcal{F}_1$

(c) $\mathcal{F}_4$

(d) [LS08]

(e) this construction

(f) [KP13]

Figure 10: **Three-sided caps.** Highlight lines of caps defined by functionals and guide surfaces for an off-center basis function for $n = 3$.

4 Construction of 3-sided caps

The failure of formula (7) to provide adequate shape when $n = 3$ calls for special treatment. By choosing to join the patches $\mathbf{p}^{\circ,k-1}$ and $\mathbf{p}^{\circ,k}$ with reparameterization

$$\rho^\circ : \quad b(u) := -(1-u)^3, \quad d(u) := -6(1-u)^3, \tag{14}$$

we resolve the G^2 constraints between the $\mathbf{p}^{\circ,k}$ and retain as independent the BB-coefficients shown in Fig. 9a as black disks. As in [KP13], the construction results in better shape when the location of the central point is provided. The algorithm sets one of the three neighbours of the star point so that their average equals the limit formula for Catmull-Clark subdivision, except for a slight, shape-wise important perturbation of γ_5.

$$\text{central point} = (1 - 3\gamma_5 - 3\gamma_6)\mathbf{c}_7 + \sum_{i=0}^{2}(\gamma_5 \mathbf{c}_5^i + \gamma_6 \mathbf{c}_6^i), \quad \gamma_5 := \frac{5}{96}, \ \gamma_6 := \frac{1}{6}, \tag{15}$$

The patches $\mathbf{p}^{\mathtt{l},k}$, $\mathbf{p}^{\mathtt{m},k}$ and $\mathbf{p}^{\mathtt{r},k}$ are fully determined by C^2 connection to the central patches $\mathbf{p}^{\circ,k}$ and by matching the (degree-raised and split) tensor-border $\mathbf{b}$. The tensor-border is not reparameterized but matched directly. This yields a C^2 join at $\mathbf{m}^k$.

Together, the construction now has 45 unconstrained BB-coefficients, all associated with $\mathbf{p}^\circ$: the coefficients $\mathbf{p}_{ij}^{\circ,k}, i > 2, j > 2$ that determine $\mathbf{p}^{\circ,k}$ where its four pieces join plus $19 - 1$ coefficients involved in

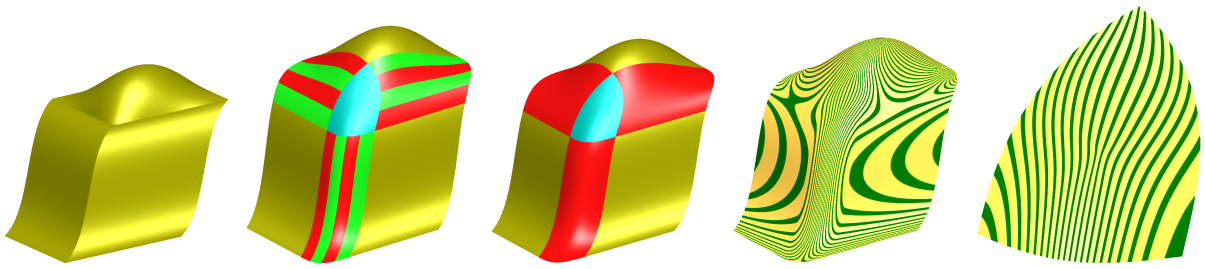

(a) input surfaces (b) bi-3 multi-blend (c) pairwise blends and cap (d) this construction (e) cap $\mathbf{p}$: this construction

Figure 11: **Three-sided caps.** (a) input surfaces of degree bi-3 (two are developable) are trimmed along parameter lines and joined C^2 pairwise by either (b) four patches of degree bi-3 or (c) one (red) blend surface of degree 3×5. The remaining three-sided hole is filled by a G^2 cap (cyan). (d,e) show highlight lines.

the G^2 constraints between $\mathbf{p}^{\circ,k-1}$ and $\mathbf{p}^{\circ,k}$. We tested a broad range of functionals including $\mathcal{F}_k$ and $\mathcal{F}_k^*$ to determine these coefficients. The best result, obtained by minimizing $\mathcal{F}_4$, is shown in Fig. 10c (together with the result of minimizing $\mathcal{F}_2 + \frac{1}{4}\mathcal{F}_1$ and the construction of [LS08]).

Since even the best choice of functional $\mathcal{F}_4$ disappoints for valence 3, we construct a **3-piece $\mathbf{G}^1$ guide** surface $\mathbf{g}$, albeit a simpler one than in [KP13]. Initially, the guide consists of three bi-5 patches (see Fig. 9c) and the patches join G^1 via a reparameterization ρ whose relevant part up to first order is defined by $a(u) := -1$ and $b(u) := 2\mathsf{c}(1-u)^2 = -(1-u)^2$. The tensor-border BB-coefficients $\mathbf{g}_{ij}^k$, $i > 2$ or $j > 2$ are defined without reparameterization by the surrounding complex and are rendered green in Fig. 9c; In particular, the bi-5 guide is C^1 connected to the surrounding complex. The G^1 constraints leave free the coefficients marked as disks, except that one additional coefficient is fixed to stabilize the central point according to (15). The remaining 14 coefficients are set by minimizing $\mathcal{F}_4$ (other functionals resulted in poorer shape). The Appendix gives the technical details of how to modify $\mathbf{g}$ to have the same layout and compatible parameterization to $\mathbf{p}$. Analogous to general case, but including the central point, we finally determine $\mathbf{p}$ when $n = 3$ by minimizing over the $45 + 1$ unconstrained coefficients the functional

$$\sum_{k=0}^{2} \sum_{s \in \{\mathsf{o},\mathsf{r},\mathsf{m},\mathsf{l}\}} \mathcal{F}_4(\mathbf{p}^{s,k} - \mathbf{g}^{s,k}). \tag{16}$$

That is, we minimize the difference between the guide $\mathbf{g}$ and the cap $\mathbf{p}$ with respect to $\mathcal{F}_4$.

We note that the choice (14) does not require reparameterizing the tensor-border so that the cap construction for $n = 3$ applies directly to tensor-borders of degree 5. By contrast, the approach of [LS08] requires a transition ring and, if the degree 3×5 blend is replaced by a sequence of bi-3 patches as in Fig. 11b, the approach of [LS08] does not apply since it requires a single cubic per half-edge. The bi-5 construction naturally fits a split boundary. (The resulting highlight line distribution is very similar to that of Fig. 11c shown in Fig. 11d,e and hence is not displayed.)

5 Further Tests

We compared and selected functionals based on a series of basic hard test cases. Here the sectors of the extended cap-net are intentionally planar in order to generate easily understood, namely zero curvature at parts of the tensor-border. (If the tensor-border has itself a complex curvature distribution, it will be more difficult to predict the expected or desirable curvature distribution of the surface cap.) Fig. 12 illustrates the effect of different choices of κ when minimizing with respect to $\mathcal{F}_\kappa$. Differences can be subtle and are best observed by moving the objects with respect to light sources. Fig. 13 and Fig. 14 compare the new construction based on minimizing functionals with those of [LS08], Catmull-Clark subdivision and [KP13]. Fig. 13 shows limitations of the otherwise good bi-7 construction of [LS08]. The highlight lines of the $\mathcal{F}_8$ construction developed in this paper and shown in Fig. 13b are more evenly distributed than of those of [LS08] but slightly less so than those of [KP13] in Fig. 13d. Applying a *single* Catmull-Clark subdivision step to make the data less extreme improves highlight lines both for [LS08] and the present algorithm. More than one step of subdivision not only increases the number of polynomial pieces but also negatively affects

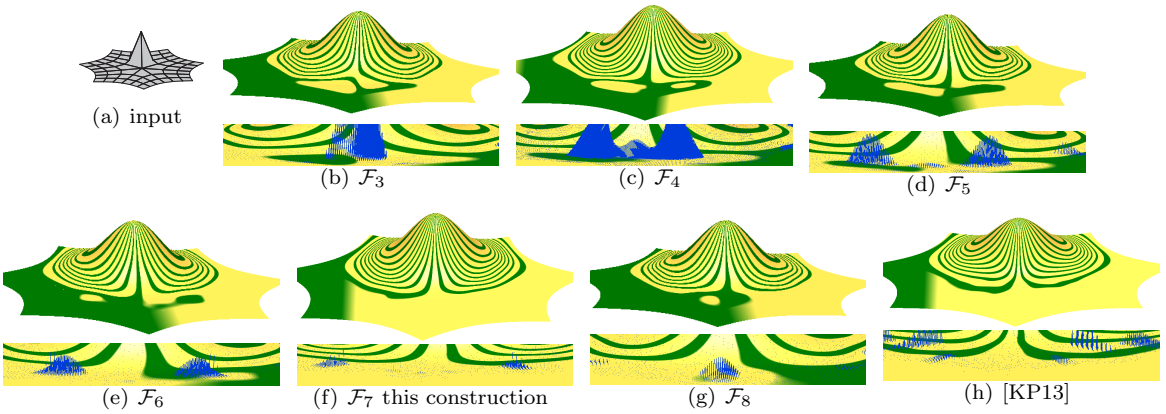

Figure 12: **Choice of functional.** Off-center basis function for $n = 7$ for the full range of functionals $\mathcal{F}_k$. The top of each image shows highlight lines, the bottom enlargement adds blue line segments pointing in the normal direction and scaled by Gauss curvature. Featuring least oscillation in front of the spike, $\mathcal{F}_7$ yields similar quality as [KP13].

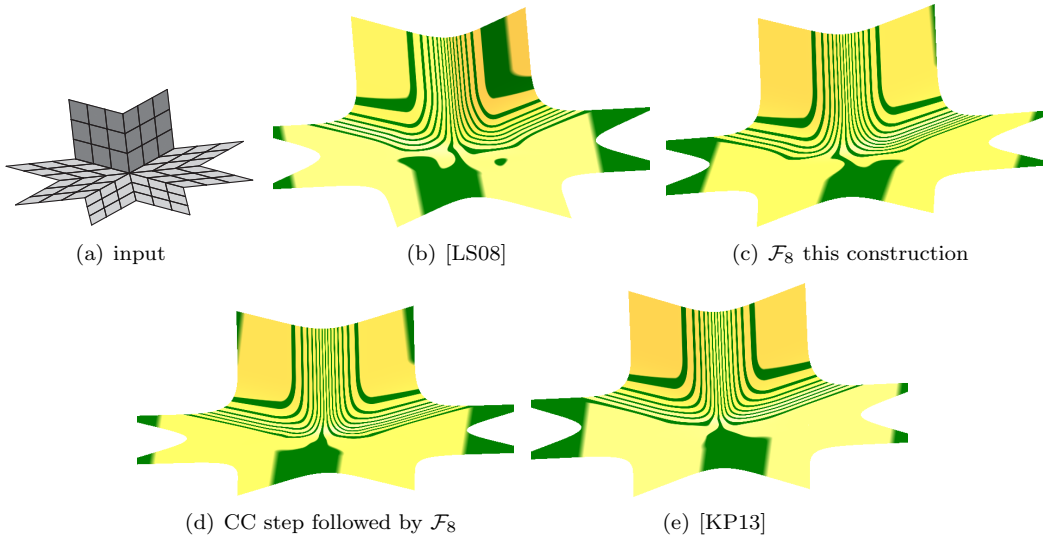

Figure 13: **Comparison with other G^2 constructions** when $n = 8$. Subtle differences are visible at the base of the transition between the vertical and the horizontal input.

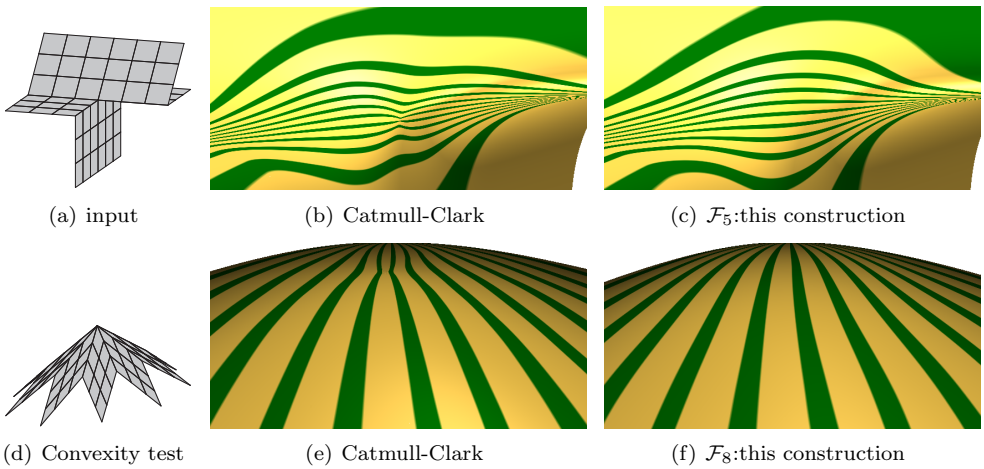

Figure 14: **Comparison with Catmull-Clark.**

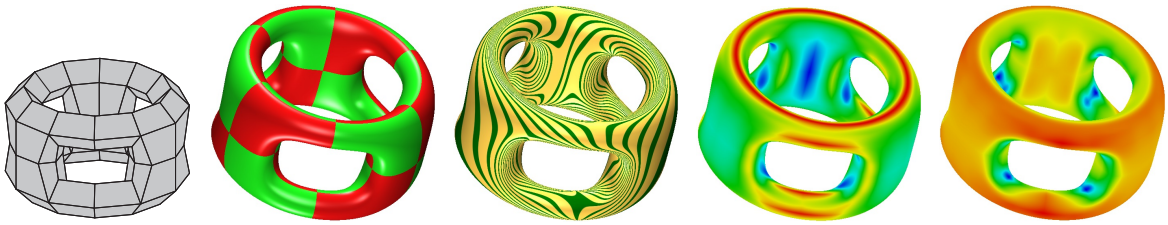

(a) input (b) 24 caps, no bi-3 (c) highlight (d) mean (e) Gauss

Figure 15: G^2 composite with adjacent caps of valence 5. (d) mean curvature, (e) Gauss curvature

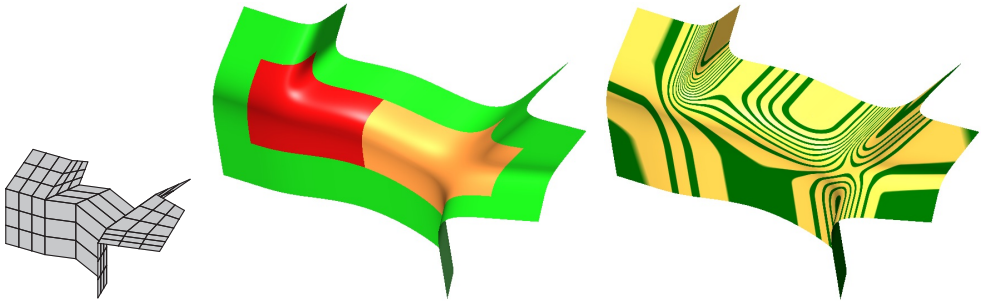

(a) input (b) adjacent caps (c) highlight lines

Figure 16: G^2 composite with adjacent caps of valence 5 and 6 of (green) bi-3 complex.

the highlight line distribution. Fig. 14 shows the artifacts of Catmull-Clark subdivision when applied to difficult saddle input and to convex input.

Fig. 15 and Fig. 16 illustrate that the construction applies and good shape is obtained also for immediately adjacent caps.

Valences above $n = 8$ are exotic in design applications. Here all functionals failed (see Fig. 17b) and, as in [KP13], we had to make the layout less distorted. In checking functionals $\mathcal{F}_k$, we can restrict k to at most the total degree 10 of the bi-5 patches – but in fact, already $\mathcal{F}_9$ turned out to be ineffective. A 3-layer construction, analogous to the one explained in [KP13], with the Catmull-Clark-like 7-partition of Fig. 17d, yields a remarkably well-distributed layout of BB-coefficients. We say remarkably, since Fig. 17d shows the BB-coefficients (uniformly scaled in the y-direction) of this (technically more elaborate) construction for $n = 1000$ on input of the tensor-border of the characteristic ring of Catmull-Clark subdivision.

6 Conclusion

Knowing that the space of bi-5 spline caps is rich enough to include caps of good shape, we applied functionals to set extraneous degrees of freedom. This approach is in contrast to relying on step-by-step improved fits via intermediate guide surfaces in [KP13]. In the cases when the valence n is greater than four, we found functionals that prevent abrupt change of the curvature distribution across the cap boundary and that gently average out the propagated highlight lines in the neighborhood of the central point. While qualitatively similar to [KP13], these constructions are conceptually simpler. For $n = 3$, we presented a guided construction of reduced complexity.

We emphasize that our choice of functionals was by elimination: functionals performing poorly on one or more of our test data sets were eliminated. One justification for choosing functionals of the form $\mathcal{F}_k$ or $\mathcal{F}_k^*$ is to assume that the surface's first fundamental form is close to the identity (see e.g. [WN01]). Then they can be interpreted as penalizing high-order terms. However, multi-sided configurations typically have ever more non-uniform parameterizations as the valence n increases, hence fail the assumption. This may explain why the degree k of the most successful functionals $\mathcal{F}_k$ selected for (11) increases with n: to obtain good shape as n and hence the complexity of the input tensor-border increases, the goal of keeping the total degree low for the whole cap must successively be abandoned.

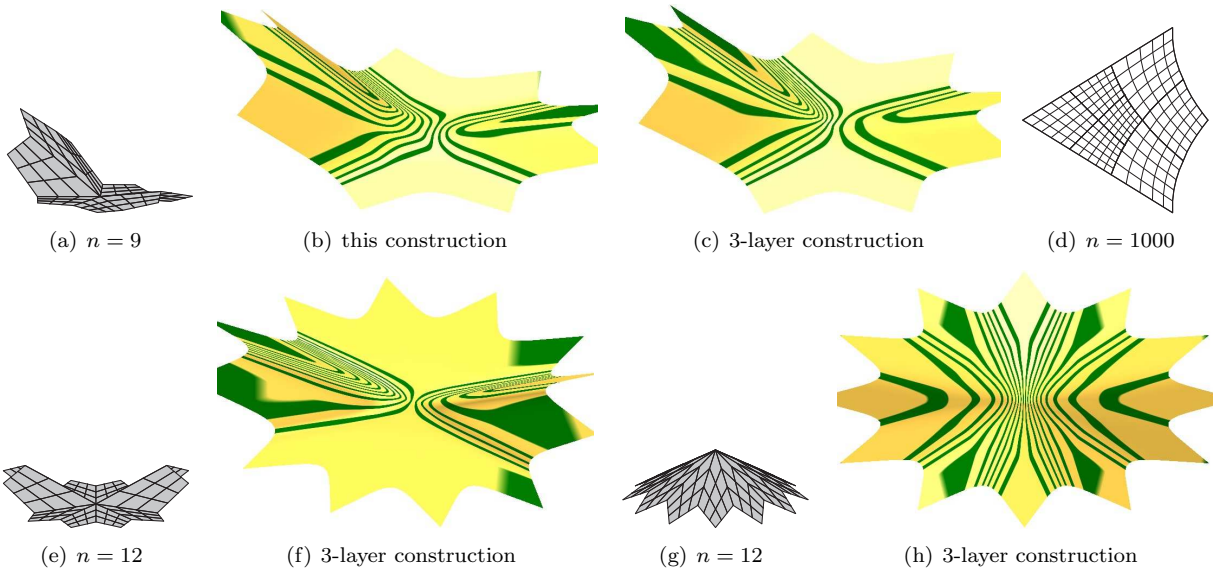

(a) $n = 9$ (b) this construction (c) 3-layer construction (d) $n = 1000$

(e) $n = 12$ (f) 3-layer construction (g) $n = 12$ (h) 3-layer construction

Figure 17: **Exotic valences** $n > 8$ require a more complex parameterization since all functionals failed for some input. (d) shows the 3-layer construction on input of the tensor-border of the Catmull-Clark characteristic ring for $n = 1000$ – re-scaled in the y-direction for better viewing.

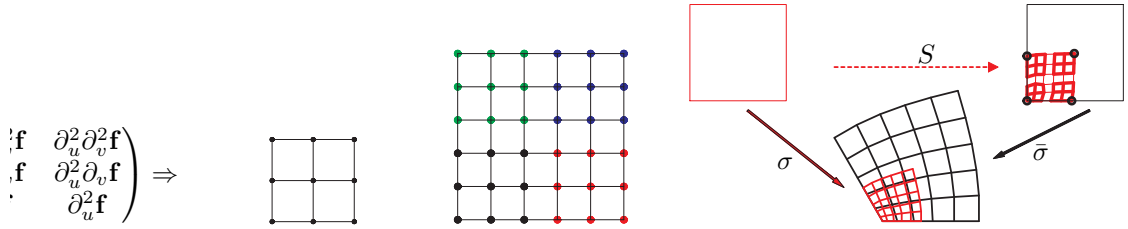

(a) Expansion of $\mathbf{f}$ (b) $H_{\mathbf{y}}\mathbf{f}$ (c) $H\mathbf{f}$ patch (d) sampling the guide

Figure 18: **BB-jet** definition (a) and BB-jet use (b,c,d). (d) bi-5 reparameterization S for sampling the bi-5 cap.

Acknowledgments.

The work was supported in part by NSF Grant CCF-1117695. Charles Loop kindly provided the generating functions for the comparisons with [LS08].

Appendix (Guide for $n = 3$)

To relate the guide to the surface cap, we found that the shape suffers if we just split $\mathbf{g}$ to obtain a patch of the same layout as $\mathbf{p}$ (see Fig. 19b vs Fig. 19c). Instead, we determine a more subtle reparameterization of the data as follows. Let $\mathbf{b}_\chi$ be the tensor-border of the characteristic ring χ of Catmull-Clark subdivision. We apply the 3-piece G^1 construction of Section 4 to $\mathbf{b}_\chi$. This yields the map $\bar{\sigma}$ of Fig. 9c. We also apply the G^2 bi-5 cap construction (without guide) to $\mathbf{b}_\chi$. This yields the parameterization σ of Fig. 9b. We now consider the BB-coefficients $\mathbf{f}_{ij}$, $i, j \in \{0, 1, 2\}$ that define the derivatives $\partial_u^i \partial_v^j \mathbf{f}$, $i, j \in \{0, 1, 2\}$, up to and including order bi-2 at a corner point $\mathbf{y}$ of the tensor-product patch $\mathbf{f} : (u, v) \in [0..1]^2 \to \mathbb{R}$ of degree bi-5 (see Fig. 18a,b) at $(0, 0)$:

$$H_{\mathbf{y}}\mathbf{f} := [\mathbf{f}_{ij}]_{i,j\in\{0,1,2\}} \tag{17}$$

We call $H_{\mathbf{y}}\mathbf{f}$ the BB-jet of $\mathbf{f}$ at $\mathbf{y}$. Fig. 18c illustrates how BB-jets at four corner points define a tensor-product patch $H\mathbf{f}$ of degree bi-5. Sampling with BB-jets, a map S of degree bi-5 for sampling the guide is obtained as follows (see Fig. 18d). We compute numerically the four vertices $S(\mathbf{y}) := (\bar{\sigma})^{-1} \circ \sigma^o(\mathbf{y})$ where $\mathbf{y} \in$

$\{(0,0),(1,0),(1,1),(0,1)\}$ and then compute the remainder of S by the requirement that $H_{\mathbf{y}}\sigma^o = H_{\mathbf{y}}\big(\bar{\sigma}\circ S\big)$. (This equation is linear for our fixed $\mathbf{y}$.) Then the central piece of the final guide with the correct layout is obtained as $\mathbf{g}^{\circ,k} \leftarrow H_{\mathbf{y}}\mathbf{g}^k \circ S$ (see Fig. 18d) and the outer pieces $\mathbf{g}^{l,k}$, $\mathbf{g}^{m,k}$, $\mathbf{g}^{r,k}$ of $\mathbf{g}$ are defined by C^2 prolongation of the tensor-border and C^2 connection to $\mathbf{g}^{\circ,k}$.

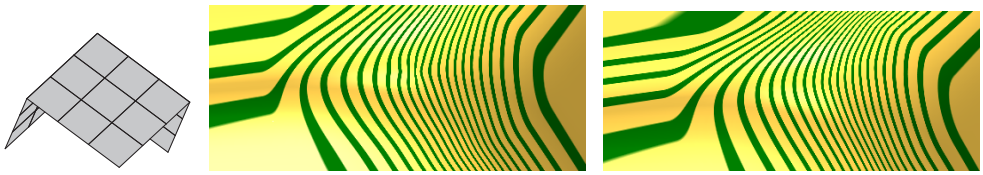

(a) input (b) without S (c) this construction using S

Figure 19: The effect of **re-sampling** via S.

References

[CC78] E. Catmull and J. Clark. Recursively generated B-spline surfaces on arbitrary topological meshes. *Computer-Aided Design*, 10:350–355, September 1978.

[CNG00] J. Cotrina Navau and N. Pla Garcia. Modelling surfaces from planar irregular meshes. *Comput. Aided Geom. Design*, 17(1):1–15, 2000.

[Far02] G. Farin. *Curves and Surfaces for Computer Aided Geometric Design: A Practical Guide*. Academic Press, San Diego, 2002.

[GH89] John A. Gregory and Jorg M. Hahn. A C^2 polygonal surface patch. *Comp Aided Geom Design*, 6(1):69–75, 1989.

[GH95] C. M. Grimm and J. F. Hughes. Modeling surfaces of arbitrary topology using manifolds. *Computer Graphics*, 29(Annual Conference Series):359–368, 1995.

[Gre94] G. Greiner. Variational design and fairing of spline surfaces. *Computer Graphics Forum*, 13(3):143–154, 1994.

[Gre96] G. Greiner. Curvature approximation with application to surface modeling. In J. Hoschek and P. Kaklis, editors, *Advanced Course on FAIRSHAPE*. B. G. Teubner, 1996.

[GZ99] John A. Gregory and Jianwei Zhou. Irregular C^2 surface construction using bi-polynomial rectangular patches. *Comp Aided Geom Design*, 16(5):423–435, 1999.

[HKD93] Mark Halstead, Michael Kass, and Tony DeRose. Efficient, fair interpolation using Catmull-Clark surfaces. In *Proc 20th Annual Conference on Computer Graphics and Interactive Techniques*, SIGGRAPH '93, pages 35–44, New York, NY, USA, 1993. ACM.

[Kic13] Przemyslaw Kiciak. Spline surfaces of arbitrary topology with continuous curvature and optimized shape. *Computer-Aided Design*, 45(2):154–167, 2013.

[KP09] K. Karčiauskas and J. Peters. Guided spline surfaces. *Comp Aided Geom Design*, 26(1):105 – 116, 2009.

[KP13] K. Karčiauskas and J. Peters. Biquintic G^2 surfaces. In G. Mullineux Robert J. Cripps and M. A. Sabin, editors, *The Mathematics of Surfaces XIV*, pages 213–236. The Institute of Mathematics and its Applications, September 2013.

[KPR04] K. Karciauskas, J. Peters, and U. Reif. Shape characterization of subdivision surfaces – case studies. *Computer Aided Geometric Design*, 21(6):601–614, july 2004.

[Lev06] Adi Levin. Modified subdivision surfaces with continuous curvature. *ACM Trans. Graph.*, 25(3):1035–1040, 2006.

[LGS99] J. Loos, G. Greiner, and H-P. Seidel. Modeling of surfaces with fair reflection line pattern. In Bob Werner, editor, *Proceedings of the International Conference on Shape Modeling and Applications (SMI-99)*, pages 256–263, Los Alamitos, CA, March 1–4 1999. IEEE Computer Society.

[Loo04] Charles Loop. Second order smoothness over extraordinary vertices. In *Symp Geom Processing*, pages 169–178, 2004.

[LS08] Charles T. Loop and Scott Schaefer. G^2 tensor product splines over extraordinary vertices. *Comput. Graph. Forum*, 27(5):1373–1382, 2008.

[PBP02] Hartmut Prautzsch, Wolfgang Boehm, and Marco Paluszny. *Bézier and B-spline techniques.* Springer Verlag, 2002.

[Pet02] J. Peters. C^2 free-form surfaces of degree (3,5). *Comp Aided Geom Design*, 19(2):113–126, 2002.

[PF09] J. Peters and Jianhua Fan. On the complexity of smooth spline surfaces from quad meshes. *Comp Aided Geom Design*, 27:96–105, 2009.

[Pra97] H. Prautzsch. Freeform splines. *Comput. Aided Geom. Design*, 14(3):201–206, 1997.

[Rei98] U. Reif. TURBS—topologically unrestricted rational B-splines. *Constr. Approx.*, 14(1):57–77, 1998.

[Sar00] Ramon F. Sarraga. A variational method to model G^1 surfaces over triangular meshes of arbitrary topology in R^3. *ACM Trans. Graph*, 19(4):279–301, 2000.

[WN01] Geir Westgaard and Horst Nowacki. Construction of fair surfaces over irregular meshes. In *Symposium on Solid Modeling and Applications*, pages 88–98, 2001.

[Ye97] Xiuzi Ye. Curvature continuous interpolation of curve meshes. *Computer Aided Geometric Design*, 14(2):169–190, 1997.

[YZ04] Lexing Ying and Denis Zorin. A simple manifold-based construction of surfaces of arbitrary smoothness. *ACM TOG*, 23(3):271–275, August 2004.